RSC Advances

ROYAL SOCIETY OF CHEMISTRY

www.rsc.org/advances

Design, Fabrication and Dielectric Properties in Core-double shell $BaTiO_3$-based Ceramics for MLCC Application

Hua Hao, [1]* Hanxing Liu, [1] Shujun Zhang, [2] Xin Shu, [1]Ting Wang, [1]Mengying Liu, [1]

Zhonghua Yao, [1]Minghe Cao[1]

1 *State Key Laboratory of Advanced Technology for Materials Synthesis and Processing, School of Material Science and Engineering, Wuhan University of Technology, Wuhan 430070, People's Republic of China*

2*Materials Research Institute, Pennsylvania State University, University Park, Pennsylvania 16802, USA*

*E-mail: haohua@whut.edu.cn Phone / Fax: 86-27-87885811

Abstract :

$BaTiO_3$-based ceramics with core-double shell structure were fabricated by precipitation and sol-gel method, respectively. $Bi(Zn_{1/2}Ti_{1/2})O_3$-$BaTiO_3$ (BZT-BT) or Nb oxide was chosen to be shell-I (inner layer) or shell-II (outer layer) composition. The structure and dielectric properties were investigated by x-ray diffraction (XRD), HRTEM (High Resolution Transmission Electron Microscopy) and electron probe micro analysis (EPMA), with different core to shell ratio (n_c/n_s). Compared with the designed composition BT-Nb-(0.2BZT-0.8BT)， BT-(0.2BZT-0.8BT)-Nb was found to possess improved dielectric temperature stability, where the capacitance variation $\Delta C/C \leqq \pm 15\%$ was achieved over temperature range of -60 ~155 ^oC, with dielectric constant and dielectric loss being on order of 1860 and 0.011 at room temperature.

Keywords : Core-double shell structure, bismuth-based perovskite, dielectric temperature stability

1.Introduction

$BaTiO_3$ (BT) is the most actively studied ferroelectric material, the mainstay for multilayer ceramic capacitor (MLCC) dielectrics in last few decades. [1-3] Forming "core-shell" structure in BT dielectric ceramics is an effective approach to improve the properties of XnR MLCC (X gives the minimum temperature of -55^{o}C, n means the maximum temperature, such as 7 for 125^{o}C and 8 for 150^{o}C, while R symbolizes percentage of the capacitance variation limit ±15% in the whole temperature range, $\Delta C/C_{25^{o}C} \leqslant \pm 15\%$). [4-7] The existence of double dielectric anomalies over the studied temperature range, which is the characteristic phenomenon of "core-shell" structure in BT ceramics, can help to improve the temperature stability of the dielectric properties. Generally, BT is the ferroelectric composition for "core" component while paraelectric oxides are the main compositions for the "shell" component. [8-10] For example, in Nb_2O_5 doped BT ceramics, the Nb^{5+} will diffuse into the crystal lattice, replacing Ti^{4+} as donor dopant and forming the chemically inhomogeneous ''core–shell'' structure [11,12], improve the temperature stability of dielectric behavior. However, chemically inhomogeneous "core-shell" structure is hard to be formed in the BT-based ceramics by traditional solid state method, due to the fact that long soaking time at sintering temperature will facilitate the oxide diffusion in the shell region. [13,14] On the contrary, wet chemical coating method, such as sol-gel or precipitation coating, is expected to increase the core-shell structure formation rate. In addition, the accumulated dielectric properties of the gradient compositions in the "core-shell" structure are dominated by both core and shell parts. [15,16] Based on the

above discussion, core-double shell structure was designed to control the dielectric properties by tuning the double shell compositions and core/shell ratio (n_c/n_s).

In our previous work, BT based ceramics with core-double shell structure have been designed, where the shell-II (outer layer) composition was bismuth-based perovskite material $Bi(Mg_{1/2}Ti_{1/2})O_3$-$BaTiO_3$ (BMT-BT) [17], fabricated by two different approaches and two-step sintering method. However, the solubility limit of the BMT composition in $xBi(Mg_{1/2}Ti_{1/2})O_3$- $(1-x)BaTiO_3$ perovskite structure is low, being only x=0.07[18], making the property tuning difficult. In this work, core-double shell structure was fabricated based on the traditional Nb-doped core-shell structure, where the $Bi(Zn_{1/2}Ti_{1/2})O_3$ -$BaTiO_3$ (BZT-BT)[19] was selected as shell-I (inner layer) or shell-II (outer layer) composition. The designed core-double shell $BaTiO_3$-based powders were prepared by sol-gel and precipitation coating methods for different shells respectively(Fig.1) and the dielectric properties of ceramics with different core/shell ratios and shell compositions were studied.

2. Experimental Procedure

xBZT-(1-x)BT ceramics were prepared by traditional solid state method. Bi_2O_3 (99.99%), ZnO (99%), $BaTiO_3$ (99.0%) and TiO_2 (99.0%) powders were batched stoichiometrically and ball milled in alcohol for 24 hours and dried, followed by calcination at 1000^{o}C for 2 hours, 5 mol% excess Bi_2O_3 was added to compensate the bismuth loss. The calcined powders were then re-milled and pressed into pellets, sintered at temperatures between 1150-1400^{o}C for 2 hours. Phase purity of the

sintered samples was determined using X-ray powder diffraction (XRD) (PANalytical X'Pert PRO).

Core-double shell structure was designed as S-1 and S-2 (Fig. 1). S-1: The composition of shell-I layer is Nb oxide, coating the BT powder (with average diameter of 400nm) by precipitation method (denoted as BT/shell-I), and the composition of shell-II layer is 0.2BZT-0.8BT which is coated BT/shell-I powder by sol-gel method (denoted as BT/shell-I/shell-II). S-2: The compositions of shell-I and shell-II layers are 0.2BZT-0.8BT and Nb oxide, respectively[20,21].

The fabrication method of 0.2BZT-0.8BT sol was as following. Firstly, $Ti(C_4H_9O)_4$ was dissolved in citric acid solution with pH value of 6. After stirring at 70 ^oC for 3h, a transparent yellow aqueous solution was obtained (named Ti sol). Then $Zn(CH_3COO)_2 \cdot 2H_2O$, $Ba(CH_3COO)_2$ and $Bi(NO_3)_3 \cdot 5H_2O$ were stoichiometrically dissolved in the acetic acid according to the nominal composition of 0.2BZT-0.8BT, and then added to the citric acid solution to help complexation reaction completely. The pH value of the obtained mixture solution was adjusted to 6~7 with ammonia solution, and a transparent aqueous solution could be achieved (refer to Bi-Zn-Ba sol). Finally, stable sol of 0.2BZT-0.8BT was obtained after stirring the mixture of Ti sol and Bi-Zn-Ba sol. On the other hand, $Nb(OH)_5$ was dissolved in 0.3mol/L oxalic acid solution to produce oxalic acid of Nb.

The procedure for S-1 was as following: the BT powder was dispersed by ultrasonic treatment about 30min in isopropanol to obtain BT slurry and then the oxalic acid of Nb compound was added to the slurry. The pH value of the slurry was

adjusted to above 5 with ammonia solution, so the Nb compound was able to precipitate completely and coat on BT particles. The dried powders were calcined at 500^{o}C for 2h to burn out the organics and obtain BT/shell-I powders. Then the BT/shell-I powder was dispersed by ultrasonic treatment about 30min in deionized water and added to the prefabricated 0.2BZT-0.8BT sol. The obtained mixture was stirred to produce a gel at 85 ^{o}C, and then dried at 120 ^{o}C to obtain xerogel. Finally, the BT/shell-I/shell-II powders were obtained by calcining the xerogel at 650 ^{o}C for 5h. The molar ratio (n_c/n_s) of the $BaTiO_3$ (core) to shell layers (including shell-I or shell-II) will affect the dielectric properties of the obtained ceramics, thus, compositions with n_c/n_s =1:1, 1:2, 1:3 and 1:4 were investigated. Compared with S-1, the procedure sequence for S-2 was adjusted according to the composition, precipitation method for Nb oxide and sol-gel method for 0.2BZT-0.8BT.

Microstructure and composition analysis of the powder and sintered samples were performed by transmission electron microscopy (TEM) and energy dispersive spectroscopy (EDS) using a JEOL JEM-2100F operated at 200 kV. The element distributions of ceramics were analyzed by Electron Probe Micro -Analyzer (EPMA, JXA-8230). The samples were polished to get parallel surfaces, and then electroded using fire-on silver paste. Dielectric measurements were carried out on samples using a multi-frequency precision LCRF meter (4184A, Agilent) in the temperature range of -60~200 ^{o}C.

3. Results and Discussions

3.1 Dielectric properties of $xBi(Zn_{1/2}Ti_{1/2})O_3$-(1-x)$BaTiO_3$ ceramics

Pure perovskite xBZT-(1-x)BT solid solution can be formed in the range of x=0.05~0.35, above which, a second phase of $Bi_4Ti_3O_{12}$ appears, revealing the solid solution limit (Fig.2). According to the peak splitting of the {200} diffraction, as shown in Fig.2b, the sample exhibits tetragonal symmetry between x=0.05~0.10, transforms to pseudo-cubic phase when x>0.1[22,23].

The dielectric constant and $\Delta C/C_{25^oC}$ as a function of temperature for xBZT-(1-x)BT ceramics at 1 kHz frequency are shown in Fig.3. With BZT content increasing, the value of the dielectric constant at room temperature is gradually decreased, accompanied by a diffused dielectric peak, giving a more smeared behavior. Meanwhile, the temperature variation of the capacitance ($\Delta C/C_{25^oC}$) was found to maintain the same trend with increasing BZT content, but with values gradually increased in the high temperature region (about 25~200 ^oC). To meet the requirement of the capacitance variation limit $\pm$15% (dash line in Fig.3 b), BZT-BT with composition of x=0.2 shows improved stability in high temperature region, demonstrating that a certain amount of BZT will benefit the capacitance stability of $BaTiO_3$ at high temperature.

Temperature variations of the capacitance for 0.2BZT-0.8BT and 0.25BZT-0.75BT ceramics were found to meet $\Delta C/C_{25^oC} \leqq \pm 15\%$ in high temperature range up to 200 ^oC, but fail at low temperature end (-55 ^oC). It should be noted both 0.2BZT-0.8BT and 0.25BZT-0.75BT ceramics exhibit wider temperature range ($\Delta C/C_{25^oC} \leqslant \pm 15\%$) when compared to other compositions (as compared in Table 1).

However, considering the values of dielectric constant and dielectric loss, the 0.2BZT-0.8BT ceramic was selected as "shell" composition for core-double shell structure.

3.2 Structure and dielectric properties of BT-based ceramics with core-double shell structure

3.2.1 S-1 specimens

TEM images of Nb-oxide coated BT powder（BT/shell-I）(n_c/n_s=1:1) by precipitation method are given in Figs. 4a &b. The domain structure of BT can be examined in the powder, as shown in Fig. 4a, around which there is an amorphous coating layer (Fig. 4b), due to the low sintering temperature (500^{o}C). The powder of 0.2BZT-0.8BT coated BT/shell-I was also analyzed by TEM, as given in Figs. 4c &d, showing an obviously thicker coating layer around the core when compared with BT/shell-I.

The EDS analysis together with TEM was performed on S-1 ceramic samples and given in Fig.5, in which the ''core–shell'' structure can be observed. To confirm the main composition of the core and shell, EDS analysis was employed on different locations (spots 1, 2, 3 and 4) of the grain, including the core and shell parts. It is obvious that the concentrations of Nb and Bi in the shell area (spot 1) are much higher than those on other spots (spots 2 and 3), corresponding to the shell- I composition, while the main composition of the core (spots 2 and 3) is $BaTiO_3$. In addition, the Ba/Ti relative concentration on spot 4 was found to be lower than those on spots 2 and 3, corresponding to shell- II composition.

3.2.2 S-2 specimens

TEM images of 0.2BZT-0.8BT coated BT powder（BT/shell-I）(n_c/n_s=1:1) are shown in Figs. 6a, &b. As observed for S-1, the BT powder has small average particles size (400nm) and large specific surface area, leading to particle agglomeration. However, domain structure of the BT (shown by the arrow in Fig.6a) can still be observed. The spacing of the lattice fringe 0.2821 nm observed by HRTEM（Fig.6b）corresponds to the (110) plane of the tetragonal BT crystal, whereas the lattice fringe 0.4644nm corresponds to the double (111) plane of the shell-I pseudo-cubic 0.2BZT-0.8BT, being in good agreement with the designed composition. In addition, the powder of Nb-oxide coated BT/shell-I was analyzed by TEM, as given in Figs. 6c &d. Similarly, particles are still in agglomeration, around which there are amorphous coating layers, with thickness being larger than that of BT/shell-I, revealing the optimized coating behavior.

S-2 ceramic samples were analyzed by TEM, as shown in Fig.7. The ‘‘core–shell’’ structure can be observed, similar to S-1, the core is ferroelectric $BaTiO_3$ with typical domain structure, while the shell is the solid solution 0.2BZT-0.8BT or Nb oxide, which is in paraelectric phase. To confirm the main compositions of the “core-shell” structure, three representative spots (corresponding to spots 1, 2 and 3) were analyzed by EDS. It is obvious that the concentrations of Bi, Zn and Nb in the core area (spot 2) are much lower than those in the shell (spot 1 and spot 3), indicating the main composition of the core is $BaTiO_3$. Meanwhile, it can be confirmed that the main compositions of the shell material follow the expectation. Nb

oxide-coating layer is the outer layer, corresponding to spot 1, where niobium and small amount of bismuth were detected, while Ba/Ti relative contents were found to decrease on spot 3 with increased bismuth concentration, revealing that the BT-BZT composition dominate the shell-I layer. Compared with S-1 ‘‘core–shell’’ structure (Fig. 5), the core component of S-2 was found to reduce, with increased shell thickness, which was expected to affect the dielectric properties.

S-2 ceramic samples were analyzed by Electron Probe Micro -Analyzer (EPMA), as given in Fig. 8, showing the distribution of Ba element. High Ba concentration was observed at some spots, as marked by the black arrows, corresponding to the core portion, whose main composition is $BaTiO_3$. The distributions of Bi and Zn were found to be higher in the area where Ba concentration was low, as shown by the white arrows in the graph.

3.3 Dielectric properties of S-1and S-2 ceramics

The dielectric constant and temperature variation of capacitance as a function of temperature for S-1 and S-2 samples with different n_c/n_s ratios are shown in Fig. 9 and Fig. 10, respectively. It was observed that the dielectric-temperature curves for both fabrication methods showed a “double peaks” effect, which is the typical feature of the “core-shell” structure. [11,24] For S-1 (Fig. 9), the dielectric peak was found to suppress at low temperature region, but enhanced gradually as the shell volume fraction decreased at high temperature region. It should be noted that there is only minimal dielectric constant variation with increasing n_c/n_s ratio. Therefore the

capacitance-temperature stability doesn't show significant improvement, regardless of the variation of n_c/n_s ratios for S-1 samples (Fig. 9b). On the contrary, dielectric constant for S-2 is sensitive to the n_c/n_s ratios, where the dielectric constant was found to increase in both low temperature and high temperature regions with improved capacitance-temperature stability, as a function of n_c/n_s ratio (Fig. 10).

The dielectric properties of the materials with a core–shell structure can be regarded as the accumulated properties of the ferroelectric core, paraelectric shell and the gradient compositions, using Lichtenechers equation $lg\varepsilon=V_c \cdot lg\varepsilon_c+V_s lg \cdot \varepsilon_s$, where V_c, and V_s are the volume ratio of the core and shell respectively, ε_c, and ε_s are the dielectric constants for the core and shell respectively. So it is expected that the dielectric properties of the ceramics could be modified by tuning the core-shell volume ratios. [25,26] Considering the diffusion between multilayers will affect the dielectric properties, 0.2BZT-0.8BT/BT and Nb-oxide/BT, were fabricated, the EPMA elemental distribution testing was employed to analyze the ion diffusion at the interfaces (Fig. 11). There is no obvious diffusion between BT and Nb-oxide interface, while there is obvious Bi diffusion from 0.2BZT-0.8BT to BT. So in S-1 samples, the major component of core is BT according to n_c/n_s ratio, leading to relative high dielectric constant peak at Curie temperature (about 4500). While in S-2, the core composition on the proximity of the 0.2BZT-0.8BT shell layer will fluctuate，leading to the reduced ferroelectric core (BT), being confirmed by TEM, as shown in Fig. 5 and Fig. 7, accounting for the decreased dielectric constant peak at Curie temperature (from 2000 to 3500, depends on the n_c/n_s ratio, Fig. 11a). The dielectric constant

corresponding to shell composition increases with n_c/n_s ratio increasing, due to the fact that the Bi diffusion make BZT component decrease correspondingly in the shell composition, leading to the increased dielectric constant. Therefore, the dielectric-temperature stability is improved for S-2 ceramics. Compared with the properties of the reported Nb-coated BT, double shells (0.2BZT-0.8BT and Nb oxides) of S-2 sample with n_c/n_s=1:1 helped to extend the temperature range meeting the requirement of the $\Delta C/C \leqq \pm 15\%$ (as summarized in Table 2).

4. Conclusions

Core-double shell structure was designed using BZT-BT and Nb oxide as different coating compositions and BT as core composition, which were named as S-1 and S-2. Different structure design gives rise to divergences in microstructure of ceramic materials, playing an important role on the dielectric properties. The ceramic samples designed as S-2 exhibit improved dielectric properties when compared to S-1, with dielectric constant and loss being on order of 1860 and 0.011 at room temperature respectively, while the $\Delta C/C \leqq \pm 15\%$ is maintained over the temperature range of -60 ~155 ^{o}C, meeting the X8R MLCC specification.

Acknowledgements

This work was supported by Natural Science Foundation of China (No.51102189，No.51372191), the program for New Century Excellent Talents in University (No.NCET-11-0685)，International Science and Technology Cooperation Program of China (2011DFA52680).

References

1 B. Tang, S. Zhang, X. Zhou, Y. Yuan, L. Yang, *J. Electroceram.*, 2010, 25(1), 93.

2 S. Liu, H. Zhang, L. Sviridov, L. Huang, X. Liu, J. Samson, D. Akins, J. Li, S. O'Brien, *J. Mater. Chem.*, 2012, 22, 21862.

3 Y. Mizuno, T. Hagiwara, H. Chazono, *J. Eur. Ceram. Soc.*, 2001, 21, 1649.

4 M. T. Buscaglia, V. Massimo, Z. Zhao, V. Buscaglia, P. Nanni, *Chem. Mater.*, 2006, 18(17), 4002.

5 H. Wen, X. Wang, Z. Gui, L. Li, *J. Electroceram.*, 2008, 21, 545.

6 S. C. Jeon, C. S. Lee, S. J. L. Kang, *J. Am. Ceram. Soc.*, 2012, 95(8), 2435.

7 H. Chazono, H. Kishi, *J.Am.Ceram.Soc.*, 2000, 83(1), 101.

8 C. Huber, T. D. Mona, C. Elissalde, F. Weill, M. Maglione, *J. Mater. Chem.*, 2003, 13, 650.

9T.Schneller, S. Halder, R. Waser, C. Pithan, J. Dornseiffer, Y.Shiratori, L. Houben, *J. Mater. Che m.*, 2011, 21, 7953.

10 R. Berthelot, B. Basly, S. Buffière, J. Majimel, *J. Mater. Chem. C*, 2014, 2, 683.

11 S.H Yoon, J.H. Lee, D.Y. Kim, N. M. Hwang, *J. Am. Ceram. Soc.,* 2003, 86 (1), 88.

12G.F. Yao, X.H. Wang, Y.C. Zhang, Z.B. Shen, L.T. Li，J. Am. Ceram. Soc., 2012, 95(11),3525.

13 D. Hennings, G. Rosenstein, *J.Am.Ceram.Soc.*, 1984, 67(4), 249.

14 B. Xiong, H. Hao, S. Zhang, H. Liu, M. Cao, Z. Yu, *Ceram. Int.*, 2012, 38S, S45.

15 L. Xie, X. Huang, C. Wu, P. Jiang, *J. Mater. Chem.*, 2011,21, 5897.

16 Z Tian, X. Wang, L. Shu. T. Wang, T. H. Song, Z. Gui, L. Li, *J.Am.Ceram.Soc.*, 2009, 92(4), 830.

17 H. Hao, H. Liu, S. Zhang, B. Xiong, X. Shu, Z. Yao, M. Cao, *Scripta Mater.*, 2012,67(5),451.

18 B. Xiong, H. Hao, S. Zhang, H. Liu, M. Cao, Z. Yu, *J.Am.Ceram.Soc.*, 2011, 94(10), 3412.

19 C. C. Huang, D. P. Cann, *J. Appl. Phys.*, 2008, 104, 24117.

20 Y. Zhang, X. Wang, J.Y. Kim Z. Tian, J. Fang, K. H. Hur, L. Li, *J.Am.Ceram.Soc.*, 2012, 95(5), 1628.

21 L. Xie , X. Huang , Y. Huang , K. Yang, P. Jiang, *J. Phys. Chem. C*, 2013, 117(44), 22525.

22 N. Triamnak, R. Yimnirun, J. Pokorny, David P. Cann, *J.Am.Ceram.Soc.*,2013, 96(10),3176.

23 C.C. Huang, D. P. Cann, J. Appl. Phys.,2008, 104(2),024117.

24 M. Cernea,B.S. Vasile, A. Boni, A. Iuga,Journal of Alloys and Compounds,2014,587,553.

25 J. S. Park, Y. H. Han,J. Eur. Ceram. Soc., 2007,27,1077.

26 Z. Li, L. A. Fredin, P. Tewari, S. A. DiBenedetto,M. T. Lanagan, M. A. Ratner, T. J. Marks, *Chem. Mater.,* 2010, 22, 5154.

27 J.J.Gan, W.J. Wei, *Int. J. Appl. Ceram. Technol.*, 2009, 6(6) 661.

Figures captions

Fig.1 Schematic core-double shell structure materials and designed compositions for S-1 and S-2

Fig.2 XRD diffraction patterns for xBZT-(1-x)BT ceramics

Fig.3 Dielectric constant (a) and $\Delta C/C_{25^oC}$ (b) as a function of temperature for xBZT-(1-x)BT ceramics at 1 kHz frequency

Fig.4 TEM micrograph of Nb-oxide coated BT powder(BT-shell-I) by precipitation method (n_c/n_s=1:1)(a,b) and 0.2BZT-0.8BT coated BT-shell-I powder by sol-gel method (n_c/n_s=1:1)(c,d)

Fig.5 TEM-EDS micrograph of S-1 ceramics (n_c/n_s=1:1)

Fig.6 TEM micrographs of 0.2BZT-0.8BT coated BT powder by sol-gel method (n_c/n_s=1:1)(a,b HRTEM) and Nb-oxide coated BT- shell-I powder by precipitation method (n_c/n_s=1:1)(c,d)

Fig.7 TEM-EDS micrograph of S -2 ceramic (n_c/n_s=1:1)

Fig.8 EPMA micrograph of ceramic surface (n_c/n_s=1:1)

Fig.9 Dielectric constant (a) and $\Delta C/C_{25^oC}$ (b) as a function of temperature for S-1 ceramics with different n_c/n_s ratio

Fig.10 Dielectric constant and $\Delta C/C_{25^oC}$ as a function of temperature for S -2 ceramics with different n_c/n_s ratio

Fig.11 Element distribution EPMA micrograph for Nb/BT and BZT-BT/BT ceramics

Table 1 Dielectric properties for xBZT-(1-x)BT at 1kHz

BZT content	T_m	Dielectric constant	Dielectric loss	$\Delta C/C_{25^oC} \leqslant \pm 15\%$ temperature range
0.10	32	2755	0.05	-7~114
0.15	45	2010	0.06	-3~165
0.20	48	1750	0.08	2~200
0.25	74	1435	0.10	6~200
0.30	92	1240	0.11	7~48
0.35	104	1100	0.11	6~45

Table 2 Dielectric properties (25 ^oC) for S -2 ceramics with different n_c/n_s and selected Nb-doped BT at 1kHz

Composition (n_c/n_s)	Dielectric constant	Dielectric loss	$\Delta C/C \leqq \pm 15\%$ Temperature range(^oC)
1:1	1860	0.011	-60~155
2:1	2095	0.016	-60~115
3:1	2375	0.016	-60~119
4:1	2260	0.022	-32~106
Nb(3mol%)coated BT	1983	0.006	-55~125 [27]
Nb(2mol%)mixed BT	1601	0.015	-55~125 [27]
Nb(0.05mol%)coated BT	1100	0.032	0 ~100 [24]

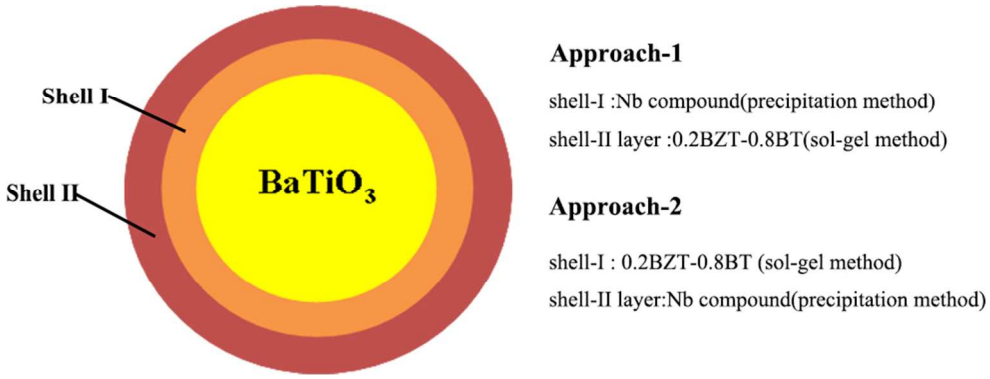

Schematic core-double shell structure materials and designed compositions for S-1 and S-2
85x31mm (300 x 300 DPI)

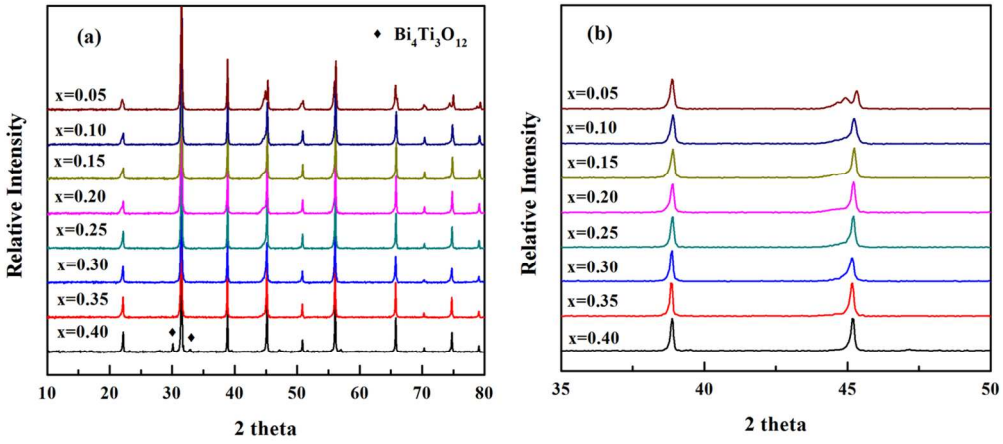

XRD diffraction patterns of xBZT-(1-x)BT ceramics
170x75mm (300 x 300 DPI)

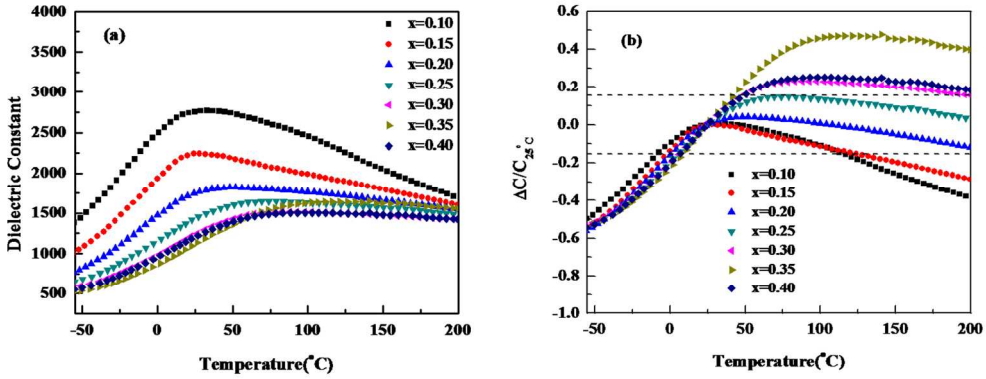

Dielectric constant (a) and ΔC/C25oC (b) as a function of temperature for xBZT-(1-x)BT ceramics at 1 kHz frequency
170x66mm (300 x 300 DPI)

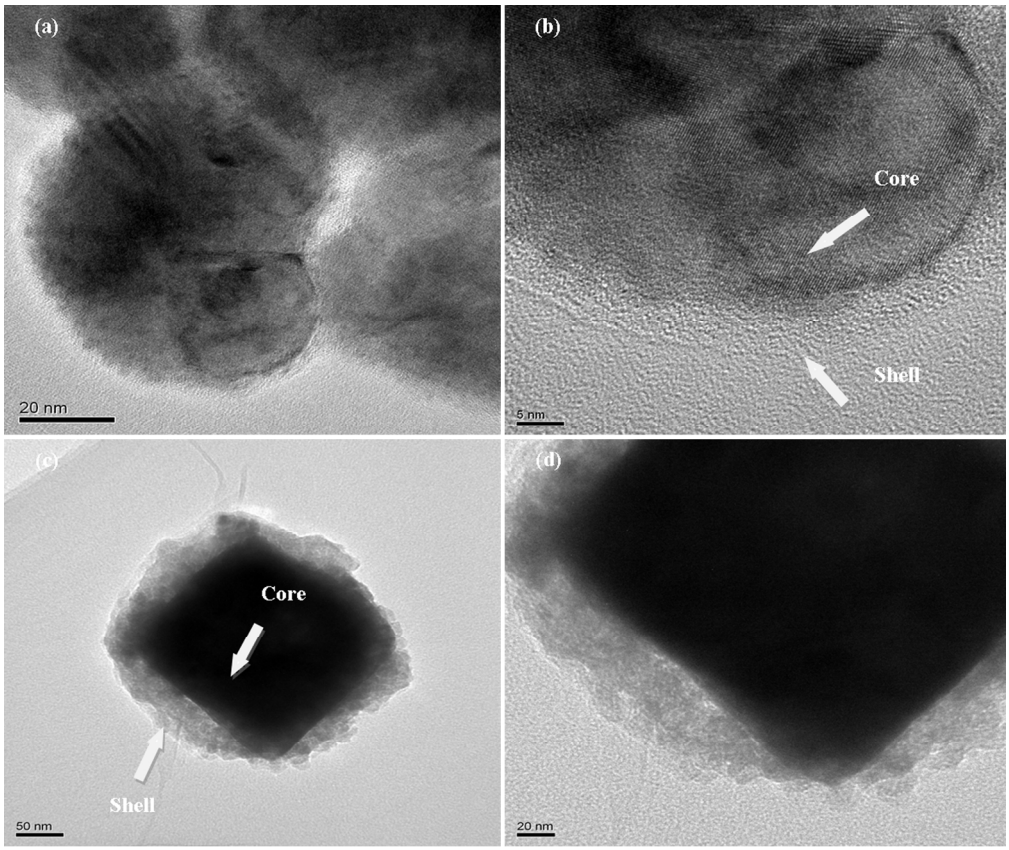

TEM micrograph of Nb-oxide coated BT powder(BT-shell-I) by precipitation method (nc/ns=1:1)(a,b) and 0.2BZT-0.8BT coated BT-shell-I powder by sol-gel method (nc/ns=1:1)(c,d)
170x143mm (300 x 300 DPI)

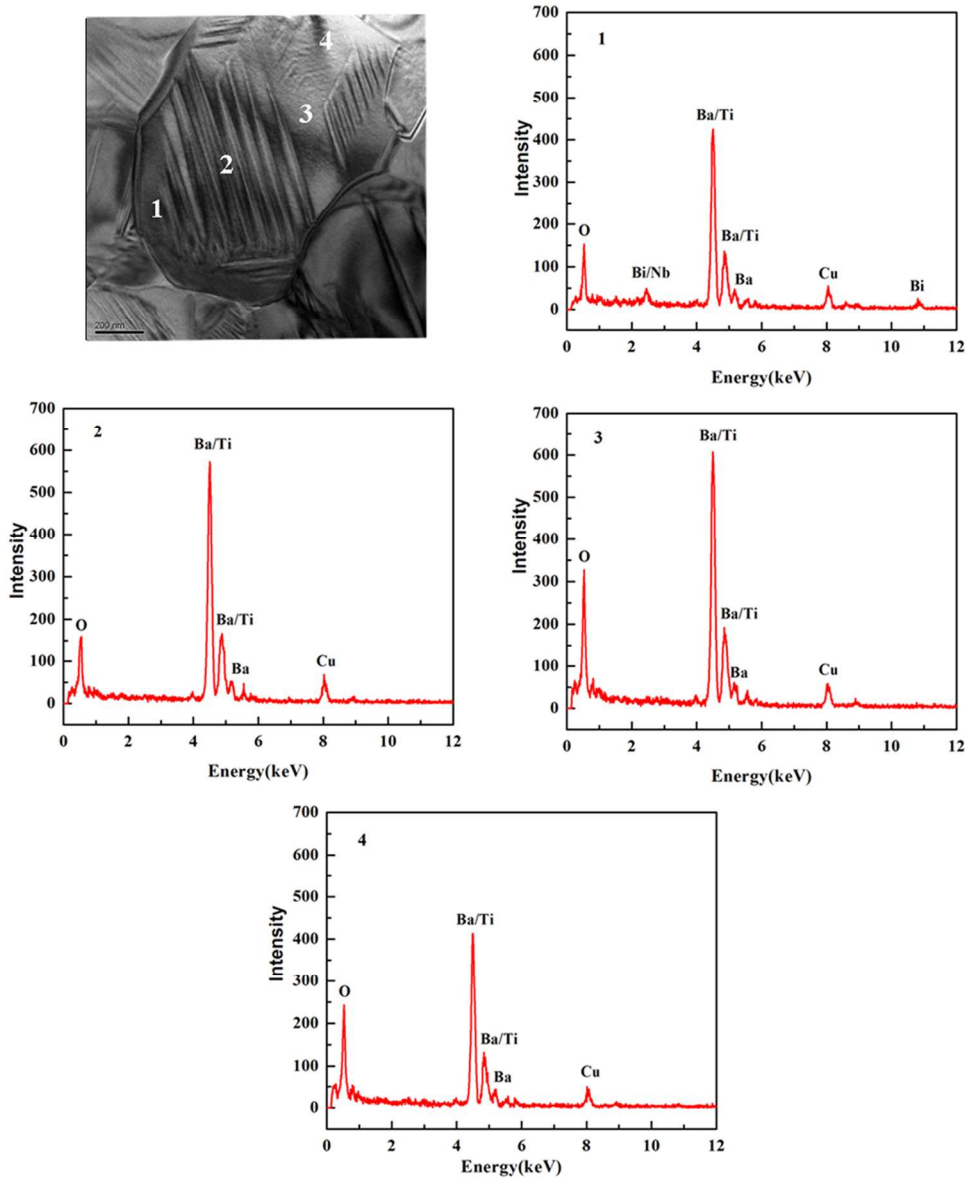

Fig.5 TEM-EDS micrograph of S-1 ceramics (nc/ns=1:1) (1, 2, 3,4 give the EDS analysis of spot 1, 2, 3,4 respectively)
170x208mm (150 x 150 DPI)

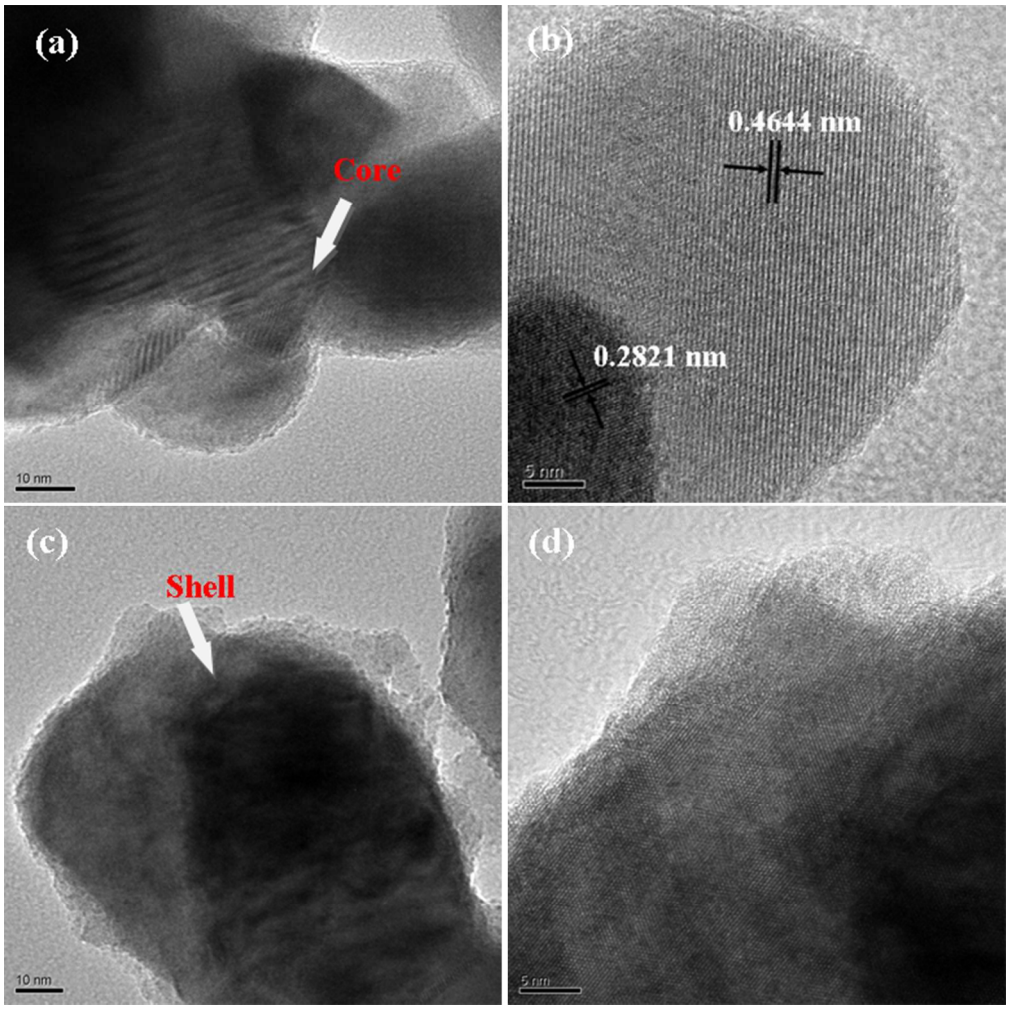

TEM micrographs of 0.2BZT-0.8BT coated BT powder by sol-gel method (nc/ns=1:1)(a,b HRTEM) and Nb-oxide coated BT- shell-I powder by precipitation method (nc/ns=1:1)(c,d)
170x169mm (300 x 300 DPI)

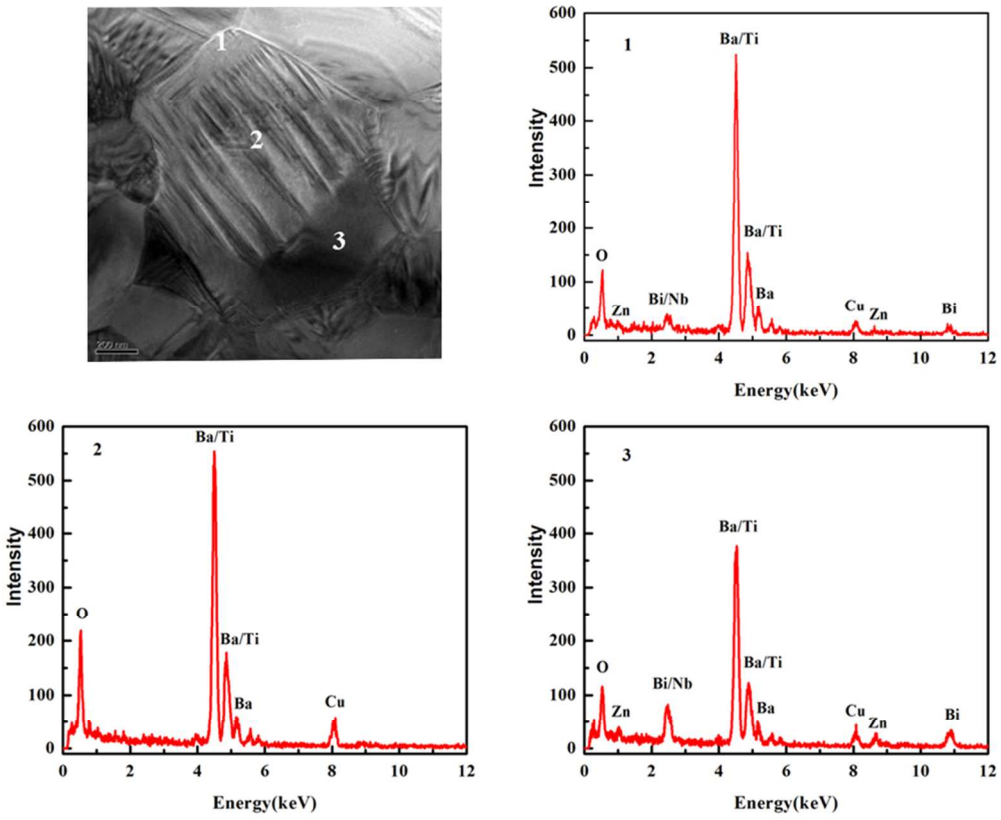

Fig.7 TEM-EDS micrograph of S -2 ceramic (nc/ns=1:1) (1, 2, 3 give the EDS analysis of spot 1, 2, 3 respectively)
170x140mm (150 x 150 DPI)

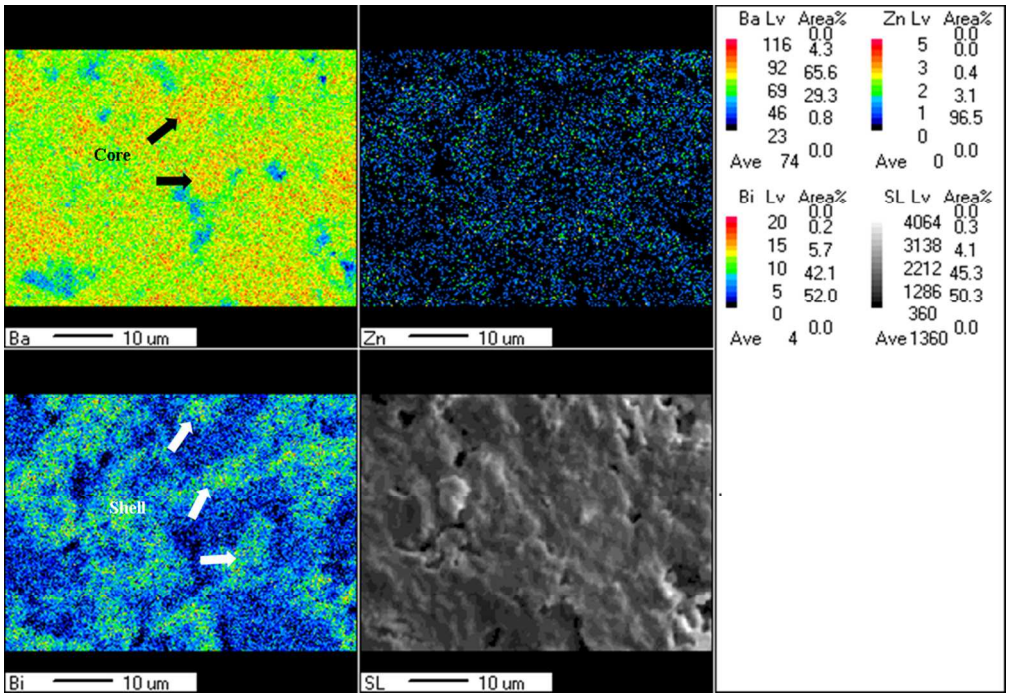

EPMA micrograph of ceramic surface (nc/ns=1:1)
170x116mm (300 x 300 DPI)

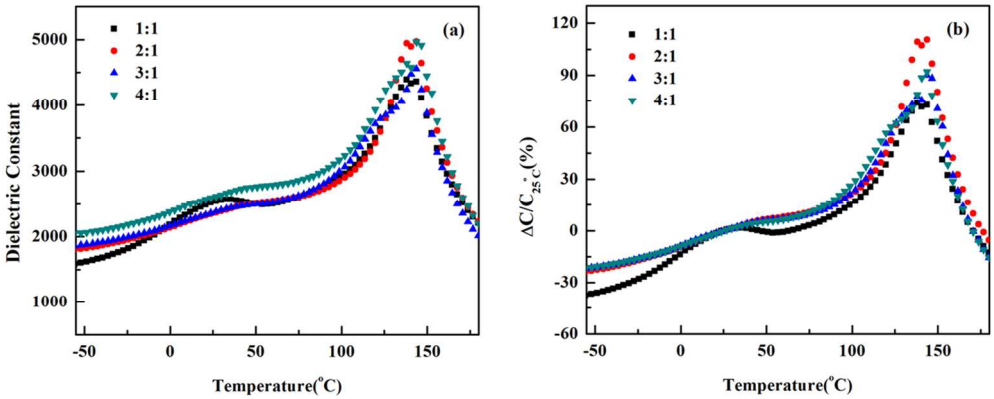

Dielectric constant (a) and ΔC/C25oC (b) as a function of temperature for S-1 ceramics with different nc/ns ratio
170x67mm (300 x 300 DPI)

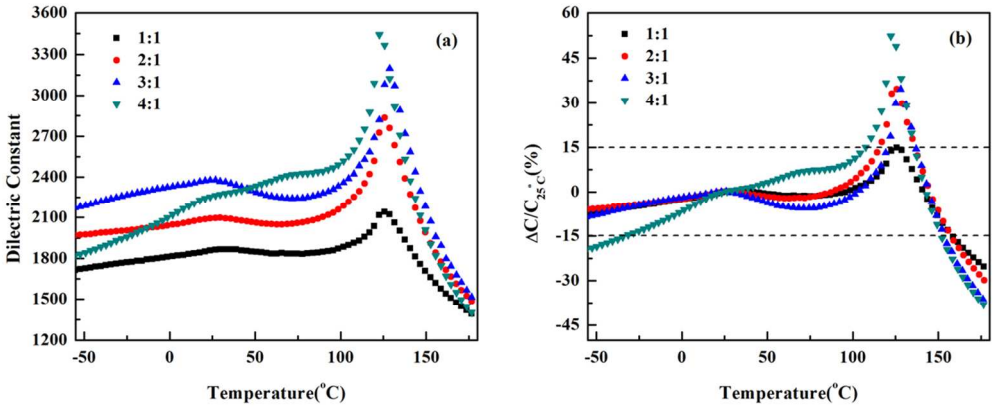

Dielectric constant and ΔC/C25oC as a function of temperature for S -2 ceramics with different nc/ns ratio
170x69mm (300 x 300 DPI)

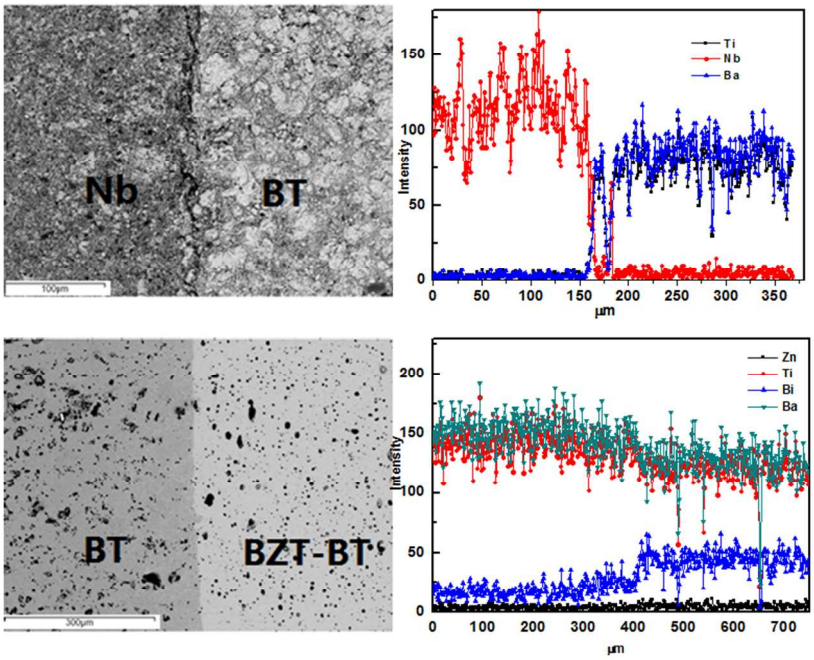

Fig.11 Element distribution EPMA micrograph for Nb/BT and BZT-BT/BT ceramics
254x190mm (96 x 96 DPI)